

Seismic and geodetic transients in Central Apennines from 2008 to 2018

Blaž Vičić¹, Abdelkrim Aoudia¹, Alessandra Borghi^{1,2}, Seyyedmaalek Momeni¹, Alessandro Vuan³

¹The Abdus Salam International Centre for Theoretical Physics, Italy

²Istituto Nazionale Geofisica e Vulcanologia, sezione di Bologna, Italy

³Istituto Nazionale di Oceanografia e Geofisica Sperimentale, Italy

Blaž Vičić (bvicic@ictp.it)

Key Points:

- Sub-horizontal shear zone beneath the shallow normal faults of Central Apennines is segmented into high and low seismicity rate subsegments.
- Well correlated seismic and geodetic transient is observed prior the 2016 Central Italy seismic sequence.
- Mw 5+ earthquakes along Campotosto fault highlight its listricity

20 **Abstract**

21 Using template matching, we investigate the space-time evolution of seismicity in the period
22 2008-2018 in Central Apennines. The seismicity appears more persistent at the base of the
23 seismogenic layer than in the shallower crust. Specifically, diffuse activity is reported on
24 Campotosto, Northern Mt. Vettore and Alto Tiberina segments at depth, alternating along strike
25 with apparent quiescence on L'Aquila, Southern Mt. Vettore and Colfiorito segments. Later
26 segments all experienced one or more Mw 6+ shallow earthquakes in 2009, 2016 and 1997
27 respectively. Central Apennines is likely underlain by a sizeable shear zone at the base of the
28 seismogenic layer with areas of diffuse seismicity bounding areas where M6+ earthquakes
29 occurred. Principal component analysis of GPS data exhibits a transient when the 2016 foreshock
30 sequence starts. This transient propagated northward from the listric Campotosto fault up to the
31 Alto Tiberina fault system and has likely loaded the Mw 6+ 2016 earthquake sequence.

32 **Plain Language Summary**

33 We use a non-standard method for the detection of microseismicity at depth for augmenting the
34 available catalog. The enhanced seismicity distribution is coupled with the observable
35 deformation on a geodetic network of continuous GPS to infer a better comprehension of the
36 earthquake behavior. The earthquake patterns in Central Apennines reveal a segmentation at
37 depth along an almost flat base of seismogenic layer with alternating low and high seismicity
38 rate segments. The deformation recorded at the surface seems to follow the seismicity variations
39 in the base of seismogenic layer along the Apenninic chain also determining a possible seismic-
40 aseismic mode. We suggest that aseismic deformation has a fundamental role in the tectonic
41 loading and that seismicity, even if heterogeneously distributed, could represent a tracer of it.
42 This conclusion is also supported by the evidence of a transient propagating from south to north
43 during the 2016 Central Italy sequence.

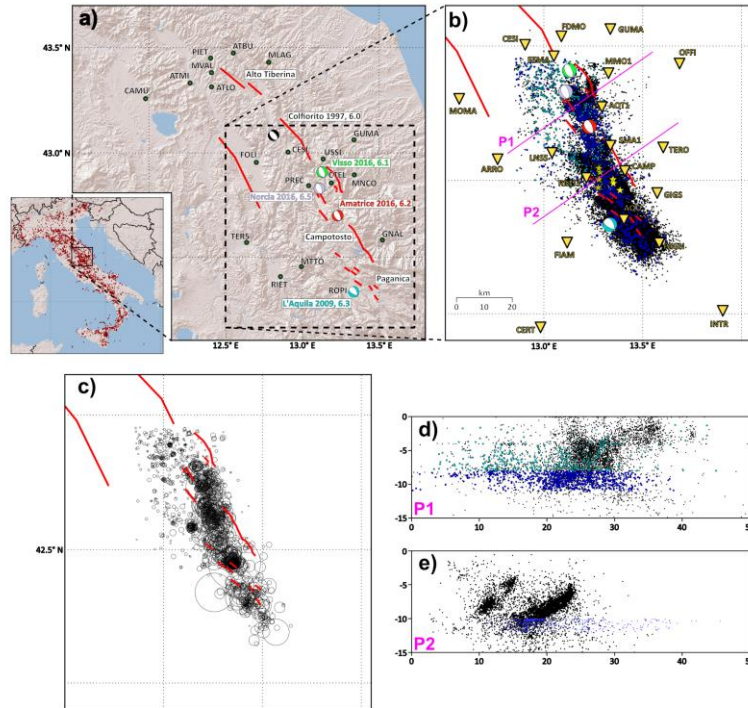
44 **1 Introduction**

45 Historical and recent destructive earthquakes in the Central Apennines, Italy (Amato et al., 1998; Rovida et al.,
46 2011; Valoroso et al., 2013; Chiaraluce et al., 2017) occur mostly along the NW-SE trending system of normal
47 faults, where approximately 2 to 3 mm/year of extension perpendicular to the mountain chain is accommodated
48 (D'Agostino et al., 2011). The system of normal faults is located above a delaminating Adria lithosphere (Aoudia et
49 al. 2007; Chimera et al., 2003) within a complex tectonic setting (eg. Doglioni, 1991; Calamita et al., 2003).

50 Central Apennines were recently struck by three destructive earthquake sequences, namely Umbria-Marche in 1997,
51 L'Aquila in 2009 and Amatrice-Visso-Norcia in 2016-2017. A large number of foreshocks and aftershocks was
52 relocated using both continuous and temporal networks (Amato et al., 1998; Chiaraluce et al., 2003; Chiaraluce et
53 al., 2011; Valoroso et al., 2013; Chiaraluce et al., 2017; Vuan et al., 2017; Improta et al., 2019) to depict the
54 geometry of the faulting system. The relocated catalogues of L'Aquila and Amatrice-Visso-Norcia sequences show
55 a sub-horizontal and gently east-dipping Shear Zone (SZ) at the base of the seismogenic zone, between 8 and 12 km.
56 The sub-horizontal geometry of SZ is confirmed by focal solutions of foreshocks and aftershocks at the base of
57 Campotosto and Monte Vettore faults (Valoroso et al., 2013; Chiaraluce et al., 2017; Improta et al., 2019).
58 Furthermore, deep seismic profiles and geologic cross-sections show a horizontal SZ between 8 and 11 km as a
59 transition from sedimentary rocks into basement units (e.g. Porreca et al. 2018). This transition corresponds to the
60 observed velocity changes underneath L'Aquila and Amatrice-Visso-Norcia sequences as inferred by local
61 earthquake travel-time tomography (Buttinelli et al. 2018; Chiarabba et al. 2018).

62 Before the L'Aquila 2009 mainshock, a foreshock sequence started in the area adjacent to the nucleation point of the
63 Mw 6.3 mainshock along the Paganica normal fault (Valoroso et al., 2013). Suga et al. (2014) identified three
64 different phases of foreshock migration towards the nucleation point of the April 6th 2009 mainshock, with one in
65 mid-February that was interpreted as a slow-slip transient. The same transient was identified using GPS data by
66 Borghi et al. (2016), who attributed it to a M6.1 slow-slip event. It was suggested that the transient took place over a
67 flat SZ at the base of Paganica and Campotosto faults involving the lateral extent of the aftershock sequence and

68 causing substantial stress loading close to the L'Aquila mainshock nucleation. Before the Amatrice, August 24th
 69 2016 earthquake, Vuan et al. (2017) on the base of newly detected foreshocks, proposed that slip along the SZ
 70 increased the stress around the source area of the mainshock, therefore contributing to the unlocking of the overlying
 71 normal faults. Furthermore, Vuan et al. (2017) reported a higher earthquake rate of foreshocks nucleating from the
 72 SZ than that of the shallower seismic activity.
 73



74
 75 *Figure 1: Studied area of Central Italy. a) Focal solutions of the recent destructive earthquakes that happened in Central Italy*
 76 *between 1997 and 2016. Red lines are their causative faults. Green dots are GPS stations used in this study. b) Triangles*
 77 *represent seismic stations used in this study. Black dots are earthquakes of the 2009 and 2016 seismic sequences, dark blue are*
 78 *selected SZ earthquakes used as templates, light blue are well located shallow earthquakes. P1 and P2 are cross sections. c)*
 79 *Circles represent the location of the template, their size corresponds to the number of near-repeaters detected by the template. d)*
 80 *Cross sections over the 2016 sequence. e) Cross section over the 2009 sequence.*

81 Among the mentioned faults, the geometry and seismic potential of the Campotosto fault (hereafter Cf) for
 82 producing large earthquakes has been a matter of debate, especially in the last decade after the occurrence of 2009
 83 and 2016-2017 events (i.e. Chiaraluca et al., 2011; Valoroso et al., 2013; Cheloni et al., 2014; Gualandi et al., 2014;
 84 Valoroso et al., 2017; Falcucci et al., 2018, Cheloni et al., 2019) (Fig. 1a), as this segment was left mostly unbroken.
 85 Cf is situated in the western flank of the Laga Mountains, oriented ~18km toward the northwest and dips toward the
 86 southwest with a listric geometry, suggested from seismic sections (Chiaraluca et al., 2011). This geometry was not
 87 retrieved from the GPS and InSAR studies (Cheloni et al., 2014, Gualandi et al., 2014, Falcucci et al., 2018, Cheloni
 88 et al., 2019) due to the quality of available data and methods used. Morpho-tectonic evidence confirms that Cf has
 89 different kinematics than its neighbor Paganica and Amatrice faults situated in its southeast and northwest,
 90 respectively, in term of fault slip rate (Falcucci et al., 2018). Cf is bounded at a depth of 10 km by SZ (Valoroso et
 91 al., 2013) and could be capable of producing an M6.4-6.6 earthquake (Falcucci et al., 2018). Two historical
 92 earthquakes on Cf were identified in study by Galadini and Galli (2003) over the past ~8 ka, each having ~1 m of
 93 minimum vertical slip. They also found that this segment did not rupture in the last 800 years based on lack of large
 94 magnitude events in historical catalogs.

95 In this study, we investigate both seismicity and deformation observed by the geodetic network of the Central
 96 Apennine fault system. We exploit waveform similarity over 11 years in the time between 2008 until the beginning
 97 of 2019 to define the spatial and temporal evolution of detected near-repeating earthquakes (cross-correlation value
 98 above 0.5) within the SZ and their relation to the reactivated normal faults. To better understand the geometry of Cf
 99 we invert the extended source ruptures of 8 moderate-magnitude ($4.4 \leq M \leq 5.4$) earthquakes that have occurred on the

100 Cf during the 2009 and 2017 sequences (Fig 1b). Finally, we perform a principal component analysis of all available
101 continuous GPS stations in the broader region of Central Apennines in the period between January 1st 2015 until
102 August 24th 2016 to detect possible geodetic transients and investigate their significance together with variations in
103 seismicity.

104 **2 Materials and Methods**

105 **2.1 Seismicity**

106 We analyse the period from 2008 to the beginning of 2019 using only well relocated foreshocks and aftershocks of
107 April 2009 (Valoroso et al., 2013) and August 2016 mainshocks (Vuan et al., 2017) (Fig 1a, b, c, d). These selected
108 events nucleated beneath the hypocenters of the mainshocks and below their respective modelled slip distribution
109 (Walters et al., 2018) at depths ranging between 10–12 km and 8–11 km for 2009 and 2016 respectively. The
110 merged earthquake catalog was used in matched filtering to detect near-repeating earthquakes and transients (Vičić
111 et al., 2019) within the SZ. Daylong waveform data of selected stations (Fig 1b) are downsampled to 20 Hz and
112 filtered between 2-8 Hz. For each event, we compute the S-wave arrival time (Krischer et al., 2015) using a suitable
113 velocity model (Herrmann et al., 2011) and trim the 3 component data in 5 seconds length waveforms centred on
114 this arrival. We extract the templates for the four closest stations. To detect new earthquakes representing the
115 templates, we apply the matched filter detection algorithm as described in Vuan et al. (2018). The selected templates
116 allowed us to detect a large number of events (Fig 1c) which were previously not reported in 2009 and 2016
117 catalogs, and also to fill the time in between the sequences over a total of 11 years.

118 **2.2 Extended source inversion**

119 We invert near-field strong motion records of 8 moderate earthquakes (magnitude $4.4 \leq M \leq 5.4$) that occurred on the
120 Cf during 2009 and 2017 sequences to study the kinematics of the ruptured areas and further constrain the geometry
121 of Cf at depth. The three-component strong motion displacement records of the Italian national strong-motion
122 network are used to estimate the rupture parameters. The elliptical sub-fault approximation method (Di Carli et al.,
123 2010; Twardzik et al., 2012; Ruiz & Madariaga, 2013; Momeni et al., 2019) is used to retrieve the robust features of
124 the ruptures. We search for each fault rupture to obtain the best waveform-fit to the observations (see Figs. A1 to A7
125 in Appendix-A) and to infer the possible change in the geometry of the Cf along both strike and dip. The details of
126 our inversions are presented in Appendix-A. The obtained source models are visualized in supplementary Material
127 (Appendix-A).

128 **2.3 GPS**

129 We perform a detailed analysis of the available continuous GPS (cGPS) stations along the Central Apennines from
130 the Alto Tiberina fault system (ATF) to the north and area of L'Aquila 2009 earthquake (Fig 1a). The 2015-2017
131 time series of the selected stations are analysed following the procedure described in Barzaghi and Borghi (2018)
132 that includes the estimate of discontinuities due to station equipment changes, seismic events, periodic signals and a
133 linear velocity term, considering the time correlation between data. The data were spatially filtered to remove
134 correlated noise using the Principal Component Analysis (PCA), as suggested by Dong et al., (2006) in order to
135 investigate the geodetic data for possible transients (Borghi et al., 2016, Gualandi et al., 2016). The methodology is
136 described in the Supplementary Material (Appendix-C).

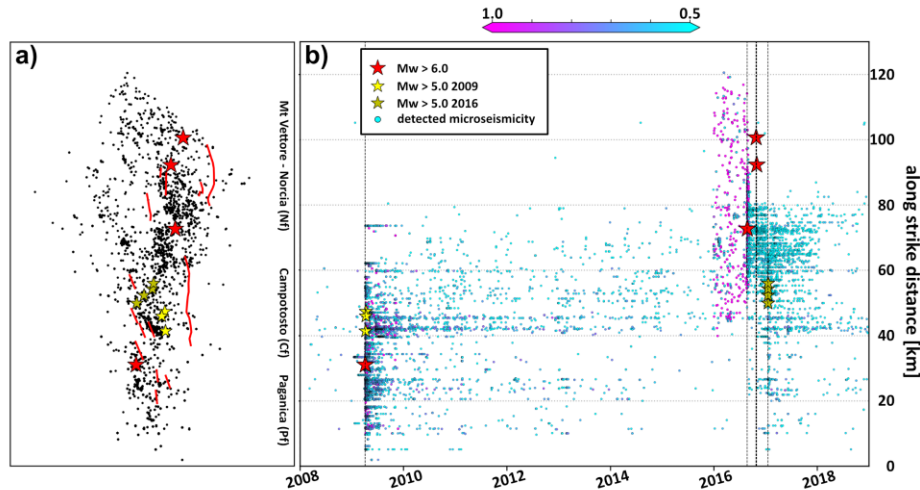
137 **3 Results**

138 **3.1 Seismicity**

139 To evaluate spatial and temporal evolution of earthquake activity within the SZ, we used 1855 templates well
140 distributed along strike and throughout the area of 2009 (10-12 km depth) and 2016-2017 (8-11 km depth)
141 sequences (Fig 2a). We analyse the continuous waveform series from 2008 to 2019, and detect 38229 near-repeaters
142 originating in the SZ, ranging between M -1.5 and M 4.7 (Supplementary Fig S2).

143 Fig 2b shows the along-strike space-time distribution of the newly detected earthquakes with cross-correlation
144 values above 0.5. For the seismicity analysis, the whole region is divided into three sub-volumes following the main
145 active faults, the Paganica fault (Pf), Cf and the Mt. Vettore-Norcia fault (Vf) (e.g. Basili et al., 2018). Diffuse and

146 continuous near-repeating earthquakes are reported within the SZ beneath Cf. Beneath Pf, the new detections exhibit
 147 a decay of aftershocks following the 2009 mainshock as in Chiaraluze et al. (2010). Beneath Vf, very few near-
 148 repeaters are detected within the SZ, except in its south-easternmost part, adjacent to Cf. We detect near-repeating
 149 earthquakes prior to the L'Aquila mainshock corresponding to the foreshock sequence of the 2009 mainshock as
 150 also reported in Sukan et al. (2014). We separate the templates of 2016 sequence into foreshock (Supplementary Fig
 151 S3a) and early aftershock templates (Supplementary Fig S3b) inherent to the August 24th Amatrice earthquake
 152 covering an 80 km along-strike distance that includes Cf and Vf. For Cf, the detection reveals a continuous rate of
 153 activity, independent of the templates we use, over the 11-year time span. For Vf, foreshock templates detect fewer
 154 events in the vicinity of Cf while on much of its extent the rate of activity is very low over about 8 years reflecting
 155 different behaviour of SZ beneath Cf and Vf.
 156



157
 158 *Figure 2: a) Locations of selected SZ earthquakes along strike the Central Italy faults activated in 2009 and 2016 sequences. b)*
 159 *Newly detected earthquakes from 2008 until the end of 2018. Color represents the cross-correlation value of the detection. 2009*
 160 *sequence undergoes a decay of seismicity along the SZ of Paganica fault while the SZ underneath Campotosto fault shows*
 161 *constant diffuse earthquake activity. At the beginning of 2016, foreshock activity of 2016 sequence start along the SZ underneath*
 162 *Campotosto fault and SZ beneath Mt. Vettore fault system.*

163 In Fig 3, detected earthquakes are plotted as a cumulative number of events over time while the yearly contributions
 164 are reported in Supplementary Material (Fig S4). We observe that soon after the 2009 mainshock and its aftershock
 165 sequence, earthquake rate within the SZ beneath Cf overtakes (September 2009) the rate beneath Pf. This is true
 166 throughout the years 2010-2015, with few exceptions when a small sequence starts along Pf (February 2011,
 167 February 2012, March 2013). The slope of earthquake rates beneath Cf seems to be stable over the years, with small
 168 increments in its rates which appear to precede sequences beneath Pf. At the end of 2015, the number of detections
 169 increased beneath Vf, starting the foreshock sequence of the August 24th 2016 Mw 6 earthquake. Beneath Cf an
 170 intensive swarm took place during February 2016, located adjacent to the future termination of the mainshock slip
 171 distribution (Chiaraluze et al., 2017). After the swarm, the SZ beneath Vf overtakes majority of earthquake rate. The
 172 aftershocks that followed the August 24th 2016 mainshock are diffuse beneath Cf and Vf, where most of the events
 173 are taking place. After the largest mainshock of October 30th 2016, the earthquake rate beneath Cf increases and by
 174 the end of 2016 seismic activity beneath Pf starts to increase. Increased activity in late December 2016 beneath Cf
 175 signals the foreshock sequence of the January 18th 2017 Mw5+ Campotosto earthquakes.

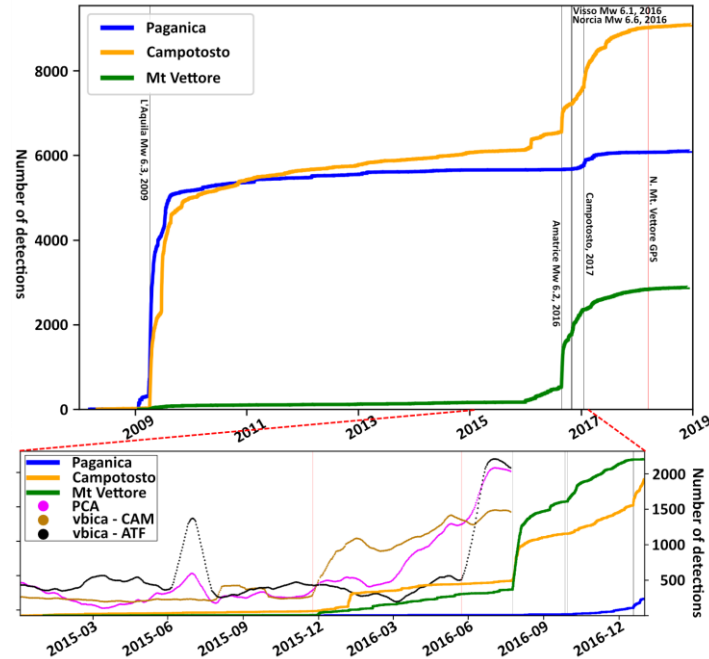


Figure 3: Cumulative number of newly detected earthquakes and a GPS transient. Different colors represent different segments of SZ under the shallow normal faults. Bottom figure shows a zoom on the beginning of 2015 until the end of 2016. Dotted pink line represents 2nd principal component over all the GPS stations used while brown and black represent independent principal component of spatially grouped GPS stations. We observe that deformation is migrating from the south of the system towards north.

176
177
178
179
180
181

182 In Supplementary material (Fig S5) we plot earthquake activity in bins of 10 km along the strike of the activated SZ
183 beneath the fault system through time. We observe a slow (6 km/year) northwestward migration of seismicity from
184 the SZ beneath Pf towards the nucleation area of the August 24th 2016 mainshock. This is followed by a
185 southeastward migration (0.2 km/day) from the August 24th 2016 nucleation area towards the hypocenters of
186 Campotosto 2017 earthquakes similar to Sebastiani et al. (2019) who observed migration of seismicity independent
187 of their depth distribution. The four Mw5+ Campotosto January 18th 2017 mainshocks appear to be trapped in
188 between 2 corridors with clusters of near-repeaters which activity intensifies starting from December 25th.

189 3.2 Rupture history for the CF moderate earthquakes

190 Seven of the studied events (except the sub-horizontal June 22nd 2009 M_L 4.4 event along SZ) occurred on planes
191 with strikes ranging from 142° to 190°, on average 157°, dipping to the southwest (Supplementary Appendix-A
192 Table A1). Our results confirm the listric geometry of Cf with dip angles changing over depth from 50° to 30°
193 (Supplementary Fig S1) as also reported by Chiaraluce et al. (2011) and Valoroso et al. (2013).

194 All obtained slip models cover an area of ~18 km per 12 km on the Cf. The patches of maximum slip of the
195 considered events do not overlap, and the ruptures evolved mostly up-dip. Similar to the migration observed along
196 the SZ after 2009 and 2016 sequence, also the 2009 and 2017 Campotosto Mw5+ ruptured patches follow a similar
197 pattern and migrate from southeast towards northwest after 2009 and vice-versa after 2016 (Fig 2d). Unilateral
198 ruptures are also confirmed by directivity observed in the accelerograms.

199 Source parameters of the 2009 sequence show an average strike of 152° and dip of 48° for the south-eastern part of
200 the Cf. We find scalar seismic moment of $1.73 \cdot 10^{17}$ Nm for the three large aftershocks and the SZ event of 2009,
201 close to the value of $1.8 \cdot 10^{17}$ Nm obtained using point source inversion method by Scognamiglio et al. (2010).
202 While using SAR and GPS data, Cheloni et al., (2014) obtained a cumulative scalar seismic moment of $3.17 \cdot 10^{17}$
203 Nm for co and post-seismic phases in 2009 and Gualandi et al., 2014 calculated an afterslip of about $2.9 \cdot 10^{17}$ Nm
204 released for 301 days after the 2009 mainshock. This information suggests that most of the deformation was
205 aseismic with half of the deformation happening as post-seismic as the sum of seismic moments released by the rest
206 of aftershocks is negligible (Falcucci et al., 2018).

207 Our obtained average strike for the 2017 events (situated on the northwestern part of the Cf) is 161° while average
208 dip angle is 35°, 13° less than Falcucci et al., (2018) from inversion of surface deformation measured from cGPS

209 and DInSAR data. We note that in their study the rake angle would play an important role in obtaining the dip angle
210 of the fault plane, while in our inversions the rake was well-retrieved parameter. The slip models distribute from
211 depths of 2.5 km to 10 km with a maximum slip of 0.49 m close to Falcucci et al., (2018) results. We obtain 7.98
212 $\times 10^{17}$ Nm of scalar seismic energy release during 2017 sequence that is close to the obtained value by Falcucci et
213 al., 2018. Considering 0.4×10^{17} Nm of scalar seismic moment released by $3.5 < M < 4.9$ aftershocks and the
214 cumulative geodetic moment of 9.29×10^{17} Nm (Cheloni et al., 2019), we reach to the same 35% contribution of
215 aseismic strain release suggested by Cheloni et al., (2019).

216 **3.3 GPS analysis**

217 The analysed GPS network is reported in Fig. 1a. The central part of the network, where the 2016 M6+ events
218 nucleated represents an empty zone since no stations were installed in that period or we do not have access to the
219 data. Although the vbICA method has resulted efficient in finding the signal along the Alto Tiberina fault (ATF)
220 (Gualandi et al., 2017), we applied the PCA method, because this method allows finding the average behavior of the
221 stations and avoids interpretation of local effects. We show the results (Fig. 3) in terms of the second Principal
222 Component (PC2) of the East component. We observe an increase of values starting at the beginning of 2016 and a
223 geographically clustered contribution of every single station to PC2. We repeat the analysis splitting the stations in
224 the northern (ATF) and in the southern part of the network. These separated analyses allowed us to point out a
225 similar behavior of the ATF and Campotosto stations but shifted in time: the Campotosto stations present this
226 discontinuity in the first vbICA component on January 7th 2016, with a probability around 94% as detected by the
227 Bayesian test inference, whereas the ATF stations present an analogous behavior seven months later on July 7th with
228 a probability of 98% (Fig 3).

229 The last analysis involves the cGPS stations that have been set up after the Mw6.5 October 30th 2016 earthquake.
230 The times-series clearly shows (Appendix-C Fig Sc3) the non-linear effect of a post-seismic deformation, so we
231 preferred to not fit the data using any functional models but performing the component analysis to describe this
232 deformation. In Appendix-C Fig Sc3 the first and second principal components are reported. All the stations are
233 affected by a common signal represented by the linear tectonic rate and the post-seismic deformations, as shown by
234 the first PC (Appendix-C Fig Sc3) but a discontinuity seems to be present at the beginning of 2018 and it is added to
235 the other signals in the first and second PC (Appendix-C Fig Sc3). Soon after, the northern extension of the area
236 affected by the 3 Mw 6+ earthquakes is hit by a series of M 3.5+ earthquakes with the strongest earthquake of M 4.5
237 on of April 10th 2018.

238 **4 Conclusions**

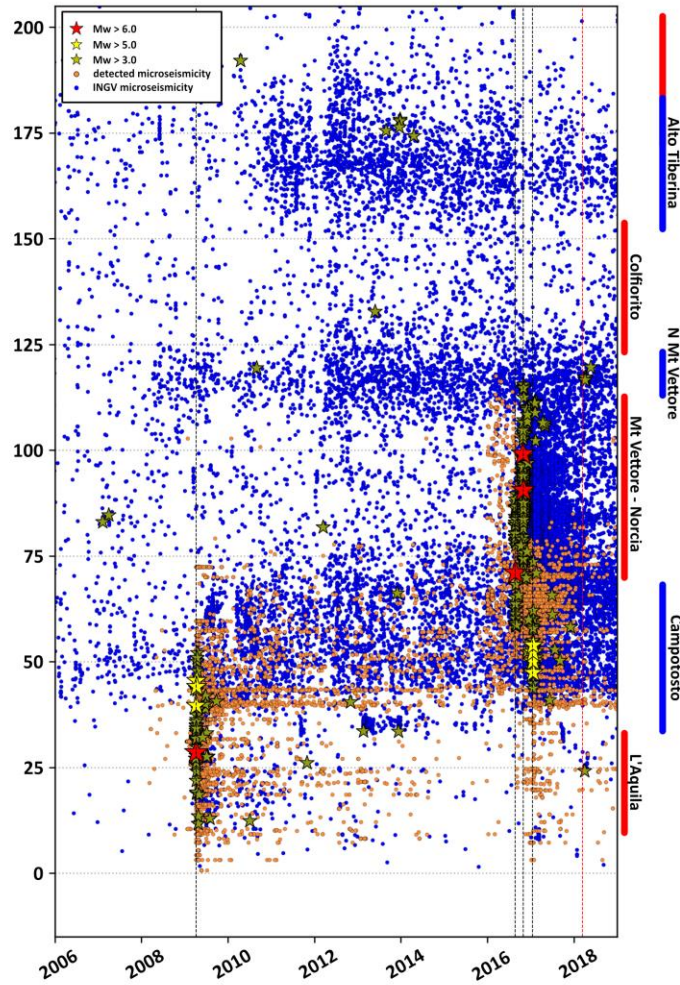
239 Analysing 11 years of continuous waveforms recorded at multiple seismic stations in Central Italy allowed us to
240 detect more than 38.000 quasi-repeaters within the SZ. The detected events and their locations give us insight on the
241 behavior in space and time of the SZ underneath Pf, Cf and Vf before, after and in-between the recent earthquake
242 sequences in Central Italy. Pf and Vf are related to the 2009 Mw 6.1 L'Aquila earthquake and to the 2016 Amatrice-
243 Visso-Norcia Mw 6+ earthquakes respectively, which ruptured shallow, SW dipping normal faults. Cf, located in
244 between Pf and Vf, is affected in the aftermath of both 2009 and 2016 sequences with earthquakes of magnitude 5+.
245 We observe different spatial and temporal patterns of earthquakes within the SZ underneath Pf, Cf and Vf.

246 The seismicity rate of the SZ appears to be segmented from south to north along the strike of the fault system (Fig
247 4). SZ beneath Pf is experiencing expected decay in its activity after the 2009 earthquake reaching a lower rate with
248 very few events after 2014 while the adjacent SZ beneath Cf exhibits a far higher rate in its activity that is
249 continuous over time.

250 The SZ beneath Vf shows a very low rate activity between 2009 up to the end of 2015 when it starts exhibiting a
251 large foreshock sequence, also affecting SZ beneath Cf and Vf as well as the above normal faults, prior to the 2016
252 Mw 6+ earthquakes.

253 The start of the foreshock sequence coincides with a clear geodetic transient that affects primarily cGPS around Cf-
254 Pf and then expands towards north on July 7th 2016 affecting cGPS around the Alto Tiberina fault. This northward
255 expansion of the geodetic transient over the fault system within 6 months mimics the northward migration of
256 seismicity within the SZ of Cf between 2009 and 2016.

257 Our results confirm the listric geometry of Cf. The comparison between the obtained co-seismic scalar seismic
258 moment and co and post-seismic release of the seismic moment by Cheloni et al., (2014) and Gualandi et al., (2014)
259 confirms the release of aseismic strain on the Cf that is also suggested by the migration of micro-events on it.



260
261
262
263
264
265
266

Figure 4: Seismicity along the strike of Central Apennines. Orange dots represents the results obtained in this study while blue dots represent earthquakes deeper than 12 km from INGV earthquake catalog. We observe good correlation between our enhanced catalog and INGV catalog. Additionally, similar behavior is observed along strike of the Central Apennines. Along the segmented SZ we observe segments of high rate seismicity (Campotosto, N. Mt. Vettore, Alto Tiberina) and segments with low rate of seismicity (L'Aquila, Mt. Vettore-Norcia, Colfiorito). Later correspond to the SZ beneath the faults, that ruptured with recent M_w 6+ events.

267
268
269
270
271
272
273
274
275
276
277
278
279
280
281

Similar behaviour as exhibited within the SZ of Pf, Cf and Vf can also be observed on the larger scale of Central Apennines. We compare our newly constrained catalog with the Italian Seismic Bulletin (Fig 4). We remove earthquakes shallower than 12 km (removing fixed depth and shallow events) and extract the events along strike of Apennines. We observe similar behavior to our own findings for the area we already explored and also NW of 2016 sequence. We observe alternating high and low seismicity rate strands along the strike of Central Apennines. The areas of last large earthquakes in 1997, 2009 and 2016 correspond to strands where seismicity is less diffuse. The high seismicity rate segments are located in between, namely Campotosto segment, North Mt. Vettore segment (NVf), and Alto Tiberina segment (Anderlini et al., 2016). Due to the different depths of events nucleating in the SZ as shown in the 2009 and 2016 sequences, SZ is not a single widespread entity underlying the Central Apennines but is segmented in depth and physical properties in the sense of low and high seismicity rate strands. The recent large events happened along the low rate portions but paleoseismology (Galadini et al., 2003, Cinti et al., 2018, Galli et al., 2019) and historic macroseismic data (Guidoboni et al., 2018) show that large events can also happen on the normal faults above the high rate strands even if much less frequent. Whether these events involve only the shallow normal faults or also portions of the SZ is beyond this paper, but the high rate segments could behave as strain reservoirs for future earthquakes.

282 SZ beneath Cf, NVf and ATF likely shows different mechanical properties than the SZ beneath Pf, Vf and Umbria-
 283 Marche zone. Our results suggest that Central Apennines is most probably underlain by a sizeable sub-horizontal
 284 shear zone that is segmented in its frictional and/or mechanical properties accommodating therefore low and high
 285 rates of seismicity at the base of the seismogenic layer. The diffuse seismicity segments at depth bound segments
 286 with apparent quiescence that are later reactivated in a cascade fashion as revealed by the 2016 sequence. The space-
 287 time correlations between the seismicity and the geodetic transient and their northward migrations are most likely
 288 patterns due to an expanding/propagating slow-slip along strike.
 289 Similar behaviour can be observed along the subduction zones, where creeping segments connect areas of future
 290 large earthquakes, after which the after-slip migrates in the previously creeping zones (Rolandone et al., 2018) and
 291 where slow-slip events can trigger megathrust earthquakes (Radiguet et al., 2016).

292 **Acknowledgments**

293 The authors would like to thank Generali group and Generali Italia for the financial support.
 294 Computations are performed at ICTP using the Argo HPC cluster. PyMPA software (Vuan et al., 2018)
 295 development is partly supported by the project “Real-time earthquake risk reduction for a resilient Europe” (RISE),
 296 a three-year project financed by the Horizon 2020 programme of the European Commission.
 297 The data to support this article are available via the European Integrated Data Archive managed by Istituto
 298 Nazionale di Geofisica e Vulcanologia (INGV) (<http://www.orfeus-eu.org/webdc3/>).

299 **References**

- 300 Amato, A., Azzara, R., Chiarabba, C., Cimini, G. B., Cocco, M., Di Bona, M., ... & Basili, A. (1998). The 1997
 301 Umbria-Marche, Italy, earthquake sequence: A first look at the main shocks and aftershocks. *Geophysical Research*
 302 *Letters*, 25(15), 2861-2864, <https://doi.org/10.1029/98GL51842>
 303
- 304 Anderlini, Letizia, Enrico Serpelloni, and Maria Elina Belardinelli. "Creep and locking of a low-angle normal fault:
 305 Insights from the Altotiberina fault in the Northern Apennines (Italy)." *Geophysical Research Letters* 43.9 (2016):
 306 4321-4329, <https://doi.org/10.1002/2016GL068604>
 307
- 308 Aoudia, A., A. T. Ismail-Zadeh, and Fabio Romanelli. "Buoyancy-driven deformation and contemporary tectonic
 309 stress in the lithosphere beneath Central Italy." *Terra Nova* 19.6 (2007): 490-495, <https://doi.org/10.1111/j.1365-3121.2007.00776.x>
 310
 311
- 312 Barberio, Marino Domenico, et al. "Hydrogeochemical changes before and during the 2016 Amatrice-Norcia
 313 seismic sequence (central Italy)." *Scientific reports* 7.1 (2017): 11735, <https://doi.org/10.1038/s41598-017-11990-8>
 314
- 315 Barzaghi, R. and A. Borghi (2018), Theory of second order stationary random processes applied to GPS coordinate
 316 time-series, *GPS Solutions* 22(3), <https://doi.org/10.1007/s10291-018-0748-4>
 317
- 318 Basili, R., Burrato, P., Fracassi, U., Kastelic, V., Maesano, F., Tarabusi, G., ... & DISS Working Group. (2018).
 319 Database of Individual Seismogenic Sources (DISS), Version 3.2. 1: A compilation of potential sources for
 320 earthquakes larger than M 5.5 in Italy and surrounding areas, <https://doi.org/10.6092/INGV.IT-DISS3.2.1>
 321
- 322 Borghi, A., L. Cannizzaro, A. Vitti (2012). Advanced techniques for discontinuities detection in GNSS coordinate
 323 time-series. An Italian case study. Proceedings of IAG 2009 Scientific Assembly "Geodesy for Planet Earth",
 324 Buenos Aires, August 31 to September 4, 2009, Springer, ISBN 978-364220337-4, https://doi.org/10.1007/978-3-642-20338-1_77
 325
 326
- 327 Borghi, A., Aoudia, A., Javed, F., & Barzaghi, R. (2016). Precursory slow-slip loaded the 2009 L'Aquila earthquake
 328 sequence. *Geophysical Journal International*, 205(2), 776-784, <https://doi.org/10.1093/gji/ggw046>
 329 Buttinelli, M., Pezzo, G., Valoroso, L., De Gori, P., & Chiarabba, C. (2018). Tectonics inversions, fault
 330 segmentation, and triggering mechanisms in the central Apennines normal fault system: Insights from high-
 331 resolution velocity models. *Tectonics*, 37. <https://doi.org/10.1029/2018TC005053>

- 332 Cinti, F. R., Civico, R., Blumetti, A. M., Chiarini, E., La Posta, E., Pantosti, D., ... & Pinzi, S. (2018). Evidence for
333 surface faulting earthquakes on the Montereale fault system (Abruzzi Apennines, central Italy). *Tectonics*, 37(9),
334 2758-2776, <https://doi.org/10.1029/2017TC004780>
335
- 336 Calamita, F., Paltrinieri, W., Pelorosso, M., Scisciani, V., & Tavarnelli, E. (2003). Inherited mesozoic architecture
337 of the Adria continental palaeomargin in the Neogene central Apennines orogenic system, Italy. *BOLLETTINO-*
338 *SOCIETA GEOLOGICA ITALIANA*, 122(2), 307-318.
339
- 340 Centamore, E., Cantalamessa, G., Micarelli, A., Potetti, M., Ridolfi, M., Cristallini, C., & Morelli, C. (1993).
341 Contributo alla conoscenza dei depositi terrigeni neogenici di avanfossa del teramano (Abruzzo settentrionale).
342 *Bollettino della Società Geologica Italiana*, 112(1), 63-81.
343
- 344 Cheloni, Daniele, et al. "Heterogeneous Behavior of the Campotosto Normal Fault (Central Italy) Imaged by InSAR
345 GPS and Strong-Motion Data: Insights from the 18 January 2017 Events." *Remote Sensing* 11.12 (2019): 1482,
346 <https://doi.org/10.3390/rs11121482>
347
- 348 Chiarabba, C., Jovane, L., & DiStefano, R. (2005). A new view of Italian seismicity using 20 years of instrumental
349 recordings. *Tectonophysics*, 395(3-4), 251-268, <https://doi.org/10.1016/j.tecto.2004.09.013>
350
- 351 Chiarabba, C., De Gori, P., Cattaneo, M., Spallarossa, D., & Segou, M. (2018). Faults geometry and the role of
352 fluids in the 2016-2017 Central Italy seismic sequence. *Geophysical Research Letters*, 45, 6963-6971.
353 <https://doi.org/10.1029/2018GL077485>
354
- 355 Chiaraluca, L., Ellsworth, W. L., Chiarabba, C., & Cocco, M. (2003). Imaging the complexity of an active normal
356 fault system: The 1997 Colfiorito (central Italy) case study. *Journal of Geophysical Research: Solid Earth*, 108(B6),
357 <https://doi.org/10.1029/2002JB002166>
358
- 359 Chiaraluca, L., Valoroso, L., Piccinini, D., Di Stefano, R., & De Gori, P. (2011). The anatomy of the 2009 L'Aquila
360 normal fault system (central Italy) imaged by high resolution foreshock and aftershock locations. *Journal of*
361 *Geophysical Research: Solid Earth*, 116(B12), <https://doi.org/10.1029/2011JB008352>
362
- 363 Chiaraluca, L., Di Stefano, R., Tinti, E., Scognamiglio, L., Michele, M., Casarotti, E., ... & Lombardi, A. (2017).
364 The 2016 central Italy seismic sequence: A first look at the mainshocks, aftershocks, and source models.
365 *Seismological Research Letters*, 88(3), 757-771, <https://doi.org/10.1785/0220160221>
366
- 367 D'Agostino, N., Mantenuto, S., D'Anastasio, E., Giuliani, R., Mattone, M., Calcaterra, S., ... & Bonci, L. (2011).
368 Evidence for localized active extension in the central Apennines (Italy) from global positioning system observations.
369 *Geology*, 39(4), 291-294, <https://doi.org/10.1130/G31796.1>
370
- 371 Di Carli, Sara, et al. "Dynamic inversion of the 2000 Tottori earthquake based on elliptical subfault
372 approximations." *Journal of Geophysical Research: Solid Earth* 115.B12 (2010),
373 <https://doi.org/10.1029/2009JB006358>
374
- 375 Doglioni, C. (1991). A proposal for the kinematic modelling of W-dipping subductions-possible applications to the
376 Tyrrhenian-Apennines system. *Terra Nova*, 3(4), 423-434, <https://doi.org/10.1111/j.1365-3121.1991.tb00172.x>
377
- 378 Dong, D., P. Fang, Y. Bock, F. Webb, L. Prawirodirdjo, S. Kedar, and P. Jamason (2006), Spatiotemporal filtering
379 using principal component analysis and Karhunen-Loeve expansion approaches for regional GPS network analysis,
380 *J. Geophys. Res.*, 111, B03405, <https://doi.org/10.1029/2005JB003806>.
381
- 382 Galadini, F., & Galli, P. (2003). Paleoseismology of silent faults in the Central Apennines (Italy): the Mt. Vettore
383 and Laga Mts. faults. *Annals of Geophysics*, <https://doi.org/10.4401/ag-3457>
384
- 385 Galli, P., et al. "The awakening of the dormant Mt Vettore fault (2016 central Italy earthquake, Mw 6.6).
386 Paleoseismic clues on its millennial silences." *Tectonics* (2019), <https://doi.org/10.1029/2018TC005326>

- 387 Gualandi, A., E. Serpelloni, and M. E. Belardinelli. "Blind source separation problem in GPS time series." *Journal*
388 *of Geodesy* 90.4 (2016): 323-341, <https://doi.org/10.1007/s00190-015-0875-4>
389
- 390 Gualandi, Adriano, et al. "Aseismic deformation associated with an earthquake swarm in the northern Apennines
391 (Italy)." *Geophysical Research Letters* 44.15 (2017): 7706-7714, <https://doi.org/10.1002/2017GL073687>
392
- 393 Guidoboni, E., Ferrari, G., Mariotti, D., Comastri, A., Tarabusi, G., Sgattoni, G., & Valensise, G. (2018).
394 CFTI5Med, Catalogo dei Forti Terremoti in Italia (461 aC-1997) e nell'area Mediterranea (760 aC-1500),
395 <https://doi.org/10.6092/ingv.it-cfti5>
396
- 397 Herrmann, R. B., Malagnini, L., & Munafò, I. (2011). Regional moment tensors of the 2009 L'Aquila earthquake
398 sequence. *Bulletin of the Seismological Society of America*, 101(3), 975-993, <https://doi.org/10.1785/0120100184>
399
- 400 Hyvarinen, Aapo. "Fast and robust fixed-point algorithms for independent component analysis." *IEEE transactions*
401 *on Neural Networks* 10.3 (1999): 626-634, <https://doi.org/10.1109/72.761722>
402
- 403 Improta, Luigi, et al. "Multi-segment rupture of the 2016 Amatrice-Visso-Norcia seismic sequence (central Italy)
404 constrained by the first high-quality catalog of Early Aftershocks." *Scientific reports* 9.1 (2019): 6921,
405 <https://doi.org/10.1038/s41598-019-43393-2>
406
- 407 Krischer, L., Megies, T., Barsch, R., Beyreuther, M., Lecocq, T., Caudron, C., & Wassermann, J. (2015). ObsPy: A
408 bridge for seismology into the scientific Python ecosystem. *Computational Science & Discovery*, 8(1), 014003,
409 <https://doi.org/10.1088/1749-4699/8/1/014003>
410
- 411 Malagnini, L., Lucente, F. P., De Gori, P., Akinci, A., & Munafo, I. (2012). Control of pore fluid pressure diffusion
412 on fault failure mode: Insights from the 2009 L'Aquila seismic sequence. *Journal of Geophysical Research: Solid*
413 *Earth*, 117(B5), <https://doi.org/10.1029/2011JB008911>
414
- 415 Mazzoli, S., Cello, G., Deiana, G., Galdenzi, S., Gambini, R., Mancinelli, A., ... & Tondi, E. (2000). Modes of
416 foreland deformation ahead of the Apennine thrust front. *Journal of GEOsciences*, 45(3-4), 246-0.
417
- 418 S M Momeni, A Aoudia, M Tatar, C Twardzik, R Madariaga, Kinematics of the 2012 Ahar–Varzaghan complex
419 earthquake doublet (M_w 6.5 and M_w 6.3), *Geophysical Journal International*, Volume 217, Issue 3, June 2019, Pages
420 2097–2124, <https://doi.org/10.1093/gji/ggz100>
421
- 422 Papadopoulos, G. A., Charalampakis, M., Fokaefs, A., & Minadakis, G. (2010). Strong foreshock signal preceding
423 the L'Aquila (Italy) earthquake (M_w 6.3) of 6 April 2009. *Natural Hazards and Earth System Sciences*, 10(1), 19-
424 24, <https://doi.org/10.5194/nhess-10-19-2010>
425
- 426 Pizzi, A., Di Domenica, A., Gallovič, F., Luzi, L., & Puglia, R. (2017). Fault segmentation as constraint to the
427 occurrence of the main shocks of the 2016 Central Italy seismic sequence. *Tectonics*, 36(11), 2370-2387,
428 <https://doi.org/10.1002/2017TC004652>
429
- 430 Porreca, M., Minelli, G., Ercoli, M., Brobia, A., Mancinelli, P., Cruciani, F., et al (2018). Seismic reflection profiles
431 and subsurface geology of the area interested by the 2016-2017 earth- quake sequence (Central Italy). *Tectonics*, 37,
432 1116- 1137. <https://doi.org/10.1002/2017TC004915>
433
- 434 Radiguet, M., et al. "Triggering of the 2014 M_w 7.3 Papanao earthquake by a slow slip event in Guerrero,
435 Mexico." *Nature Geoscience* 9.11 (2016): 829, <https://doi.org/10.1038/ngeo2817>
436
- 437 Rolandone, F., Nocquet, J. M., Mothes, P. A., Jarrin, P., Vallée, M., Cubas, N., ... & Font, Y. (2018). Areas prone to
438 slow slip events impede earthquake rupture propagation and promote afterslip. *Science advances*, 4(1), eaao6596,
439 <https://doi.org/10.1126/sciadv.aao6596>
440
- 441 Rovida, A., Camassi, R., Gasperini, P., & Stucchi, M. (2011). Catalogo parametrico dei terremoti italiani,
442 <https://doi.org/10.13127/CPTI/CPTI15.2>

- 443 Silverii, Francesca, et al. "Transient crustal deformation from karst aquifers hydrology in the Apennines (Italy)." *Earth and Planetary Science Letters* 506 (2019): 23-37, <https://doi.org/10.1016/j.epsl.2018.10.019>
- 444
- 445
- 446 Ruiz, S., and R. Madariaga. "Kinematic and dynamic inversion of the 2008 Northern Iwate earthquake." *Bulletin of the Seismological Society of America* 103.2A (2013): 694-708, <https://doi.org/10.1785/0120120056>
- 447
- 448
- 449 Soldati, G., Zaccarelli, L., Faenza, L., & Michelini, A. (2015). Monitoring of crustal seismic velocity variations in the L'Aquila fault zone inferred from noise cross-correlation. *Geophysical Journal International*, 202(1), 604-611, <https://doi.org/10.1093/gji/ggv172>
- 450
- 451
- 452
- 453 Suga, M., Kato, A., Miyake, H., Nakagawa, S., & Vuan, A. (2014). The preparatory phase of the 2009 Mw 6.3 L'Aquila earthquake by improving the detection capability of low-magnitude foreshocks. *Geophysical Research Letters*, 41(17), 6137-6144, <https://doi.org/10.1002/2014GL061199>
- 454
- 455
- 456
- 457 Twardzik, C., et al. "Robust features of the source process for the 2004 Parkfield, California, earthquake from strong-motion seismograms." *Geophysical Journal International* 191.3 (2012): 1245-1254, <https://doi.org/10.1111/j.1365-246X.2012.05653.x>
- 458
- 459
- 460
- 461 Valoroso, L., Chiaraluce, L., Piccinini, D., Di Stefano, R., Schaff, D., & Waldhauser, F. (2013). Radiography of a normal fault system by 64,000 high-precision earthquake locations: The 2009 L'Aquila (central Italy) case study. *Journal of Geophysical Research: Solid Earth*, 118(3), 1156-1176, <https://doi.org/10.1002/jgrb.50130>
- 462
- 463
- 464
- 465 Vičić, B., Aoudia, A., Javed, F., Foroutan, M., & Costa, G. (2019). Geometry and mechanics of the active fault system in western Slovenia. *Geophysical Journal International*, 217(3), 1755-1766, <https://doi.org/10.1093/gji/ggz118>
- 466
- 467
- 468
- 469 Vuan, A., Suga, M., Chiaraluce, L., & Di Stefano, R. (2017). Loading rate variations along a midcrustal shear zone preceding the Mw6.0 earthquake of 24 August 2016 in Central Italy. *Geophysical Research Letters*, 44(24), <https://doi.org/10.1002/2017GL076223>
- 470
- 471
- 472 Vuan, A., Suga, M., Amati, G., & Kato, A. (2018). Improving the Detection of Low-Magnitude Seismicity Preceding the Mw 6.3 L'Aquila Earthquake: Development of a Scalable Code Based on the Cross Correlation of Template Earthquakes. *Bulletin of the Seismological Society of America*, 108(1), 471-480, <https://doi.org/10.1785/0120170106>
- 473
- 474
- 475
- 476
- 477 Walters, R. J., Elliott, J. R., D'agostino, N., England, P. C., Hunstad, I., Jackson, J. A., ... & Roberts, G. (2009). The 2009 L'Aquila earthquake (central Italy): A source mechanism and implications for seismic hazard. *Geophysical Research Letters*, 36(17), <https://doi.org/10.1029/2009GL039337>
- 478
- 479
- 480
- 481 Walters, R. J., Gregory, L. C., Wedmore, L. N. J., Craig, T. J., McCaffrey, K., Wilkinson, M., ... & Iezzi, F. (2018). Dual control of fault intersections on stop-start rupture in the 2016 Central Italy seismic sequence. *Earth and Planetary Science Letters*, 500, 1-14, <https://doi.org/10.1016/j.epsl.2018.07.043>
- 482
- 483